JGR Atmospheres

RESEARCH ARTICLE
10.1029/2022JD037772

Regime-Specific Cloud Vertical Overlap Characteristics From Radar and Lidar Observations at the ARM Sites

Kelly A. Balmes[1,2], Joseph Sedlar[1,2], Laura D. Riihimaki[1,2], Joseph B. Olson[3], David D. Turner[3], and Kathleen Lantz[2]

[1]Cooperative Institute for Research in Environmental Sciences, University of Colorado Boulder, Boulder, CO, USA, [2]NOAA Global Monitoring Laboratory, Boulder, CO, USA, [3]NOAA Global Systems Laboratory, Boulder, CO, USA

Key Points:

- Decorrelation length scales varied by cloud regime at the Atmospheric Radiation Measurement Program Southern Great Plains site between 0.04 and 4.58 km
- Decorrelation length scales varied by site with values ranging from near 1 km in the Arctic to near 3 km in Brazil
- Decorrelation length scales for the same cloud regime across the sites were similar, although some cloud regimes exhibited differences

Correspondence to:

K. A. Balmes,
kelly.balmes@noaa.gov

Citation:

Balmes, K. A., Sedlar, J., Riihimaki, L. D., Olson, J. B., Turner, D. D., & Lantz, K. (2023). Regime-specific cloud vertical overlap characteristics from radar and lidar observations at the ARM sites. *Journal of Geophysical Research: Atmospheres*, *128*, e2022JD037772. https://doi.org/10.1029/2022JD037772

Received 1 SEP 2022
Accepted 24 FEB 2023

Abstract Climate and numerical weather prediction models require assumptions to represent the vertical distribution of subgrid-scale clouds, which have radiative transfer implications. In this study, nearly 25 years of ground-based radar and lidar observations of vertical cloud profiles at the Atmospheric Radiation Measurement Program (ARM) Southern Great Plains (SGP) site are utilized to derive cloud vertical overlap characteristics from the Cloud Type (CLDTYPE) data product. The cloud vertical overlap characteristics are further separated by cloud regime by considering seven cloud types (i.e., low cloud, congestus, deep convection, altocumulus, altostratus, cirrostratus, and cirrus) as well as periods of shallow cumulus. The decorrelation length scale (i.e., exponential transition from maximum to random overlap with layer separation) is found to vary by cloud regime, ranging between 0.04 km for cirrostratus paired with cirrus to 4.58 km for low cloud paired with cirrus at SGP. Cloud vertical overlap characteristics are also considered for other ARM sites including the Tropical Western Pacific (TWP), North Slope of Alaska (NSA), and Eastern North Atlantic (ENA) sites among other shorter term ARM deployments globally. The decorrelation length scale ranged globally from 1.03 km in the Arctic Ocean to 3.06 km in Manacapuru, Brazil. Globally, the decorrelation length scale by cloud regime exhibited similarities (e.g., for cirrus paired with cirrus) and differences (e.g., congestus paired with cirrus). The results could help inform development of cloud vertical overlap assumptions within operational numerical weather prediction models and potentially improve prediction of radiative fluxes for weather, climate, and renewable energy forecasting.

Plain Language Summary The complexity of cloud vertical structure requires approximations in weather and climate models, which has implication for the forecast of how much sunlight reaches the surface. Cloud observations from radars and lidars help to inform how cloud layers overlap vertically. The cloud observations ultimately inform what model assumptions best capture the observed cloud vertical structure. In this study, cloud profiles from ground-based radars and lidars are considered to calculate cloud vertical overlap characteristics at 18 long-term and short-term sites across the globe. The cloud vertical overlap characteristics are also considered by cloud types to understand if cloud type provides additional information on the model assumptions to use. The cloud vertical overlap characteristics are found to vary by site, season, and cloud type. The results could help inform development of cloud vertical overlap assumptions within weather and climate models and potentially improve prediction of sunlight reaching the surface, which has implications for weather, climate, and renewable energy forecasting.

1. Introduction

The vertical distribution of clouds and their representation in numerical weather and climate modeling are important for modeling and forecasting the radiative budget (e.g., Chen et al., 2000; Liang & Wang, 1997; Morcrette & Fouquart, 1986; Morcrette & Jakob, 2000; Slingo & Slingo, 1991; Stubenrauch et al., 1997; Wu & Liang, 2005). Models that do not resolve clouds (i.e., models with horizontal grid spacing larger than approximately 100 m) dictate that assumptions are required to represent the vertical distribution of clouds within the model. The vertical distribution of subgrid-scale clouds is described in weather and climate models using cloud vertical overlap methods. Cloud vertical overlap methods describe how cloud layers are vertically aligned, which is commonly described as overlapping randomly or maximally as well as combinations of maximum and random overlap (e.g., maximum-random) (e.g., Chou et al., 1998; Geleyn & Hollingsworth, 1979; Hogan & Illingworth, 2000; Tian & Curry, 1989). When cloud layers are maximally overlapped such that the total cloud fraction is minimized, this is referred to as "maximum overlap." In contrast, randomly overlapping cloud layers are referred

to as "random overlap." Minimally overlapping cloud layers that lead to maximizing the total cloud fraction is referred to as "minimum overlap." In addition, the combination of maximum and random overlap referred to as "maximum-random overlap" is another method where vertically continuous clouds are considered to be maximally overlapped and cloud layers separated by clear-sky are considered to be randomly overlapped. Another component of subgrid-scale cloud variability is the horizontal variability of cloud condensate, which are also described by overlap methods (e.g., Oreopoulos et al., 2012; Pincus et al., 2005; Räisänen et al., 2004).

Observations afford the opportunity to investigate and develop assumptions for cloud vertical overlap methods. Observations such as vertical profiles of clouds from ground-based radars (e.g., Hogan & Illingworth, 2000; Li et al., 2019; Mace & Benson-Troth, 2002; Naud et al., 2008; Oreopoulos & Norris, 2011) and satellite-based radars (e.g., Oreopoulos et al., 2012; Tian & Curry, 1989) have been used to characterize cloud vertical distribution. By utilizing cloud radar observations, Hogan and Illingworth (2000) found that observations of vertically continuous clouds followed an exponential relationship such that the cloud layers' overlap transitioned from maximum to random overlap with increasing cloud layer separation. They also found that vertically noncontinuous clouds exhibited random overlap. The combination of these two observed phenomena is referred to as exponential-random overlap. The exponential equation that describes the cloud vertical overlap distribution includes a characteristic decorrelation length scale that describes the e-folding distance for cloud layer separation where the overlap parameter is $1/e$ of maximum overlap. Shonk and Hogan (2010) explored the effect of the exponential-random overlap on the global radiative budget and found that the shortwave (SW) cloud radiative effect was changed by ~ -4 W m^{-2} compared to assuming maximum-random overlap, which highlights the importance of capturing cloud vertical overlap within models.

The high-quality ground-based measurements operated by the Atmospheric Radiation Measurement Program (ARM) sites (Ackerman & Stokes, 2003; Turner & Ellingson, 2016) provide the opportunity to investigate cloud vertical overlap characteristics from long-term cloud radar and lidar measurements. Previous studies have leveraged the capabilities of the ARM sites to investigate cloud vertical overlap characteristics including Mace and Benson-Troth (2002), Naud et al. (2008), Oreopoulos and Norris (2011), and Li et al. (2019). In this study, we expand on these studies by investigating the decorrelation length scale at the ARM Southern Great Plains (SGP) site (Sisterson et al., 2016) from nearly 25 years of observations as well as extending the sites considered to include all long-term and short-term ARM deployments that had cloud radar and lidars and the associated data products. In addition to extending the cloud vertical overlap analysis to new locations, this study will also consider the cloud type classifications from Lim et al. (2019) to help inform how the decorrelation length scale varies by cloud type, where cloud type is otherwise referred to as cloud regime. By considering cloud-regime-specific decorrelation length scales, this can help inform if decorrelation length scale specification by cloud type in weather and climate forecasting provides improvement in modeling cloud vertical distribution as well as radiative fluxes.

Section 2 describes the cloud observations from radar and lidar. Section 3 details the methods employed to derive cloud vertical overlap characteristics. Section 4 explores the impact of the decorrelation length scale on the surface radiative budget. Section 5 presents the decorrelation length scale results for the SGP site and other ARM sites considered for all cloud types and separated into contributions from different cloud types. Section 6 summarizes and presents concluding remarks.

2. Data

The ARM Cloud Type (CLDTYPE) value-added product (VAP) (Flynn et al., 2017; Lim et al., 2019) is utilized to derive cloud vertical overlap characteristics. The CLDTYPE data product provides vertical profiles of clouds and cloud type classification based on radar and lidar retrievals. The retrieval algorithm ingests the Active Remote Sensing of Cloud Layers (ARSCL) data product (Clothiaux et al., 2001; Kollias et al., 2016) from the millimeter cloud radar (MMCR) and more recently the Ka-band ARM Zenith radar (KAZR) with additional information from the micropulse lidar (MPL). The cloud boundaries from ARSCL are then categorized into cloud types based on cloud base height, top height, and geometric depth. The seven different cloud types include (a) low clouds, (b) congestus, (c) deep convection, (d) altocumulus, (e) altostratus, (f) cirrostratus/anvil, and (g) cirrus. The cloud base height, top height, and geometric depth criteria for each cloud type at the SGP site are provided in Table 1 of Lim et al. (2019). The temporal resolution is 1 min for the CLDTYPE data product.

In this study, the primary analysis will focus on the CLDTYPE data product at the ARM SGP site located in Lamont, Oklahoma (36.61°N, 97.49°W). The time period is nearly 25 years from November 1996 to September 2021. Beyond the SGP site, the CLDTYPE data product is considered at four additional sites including the

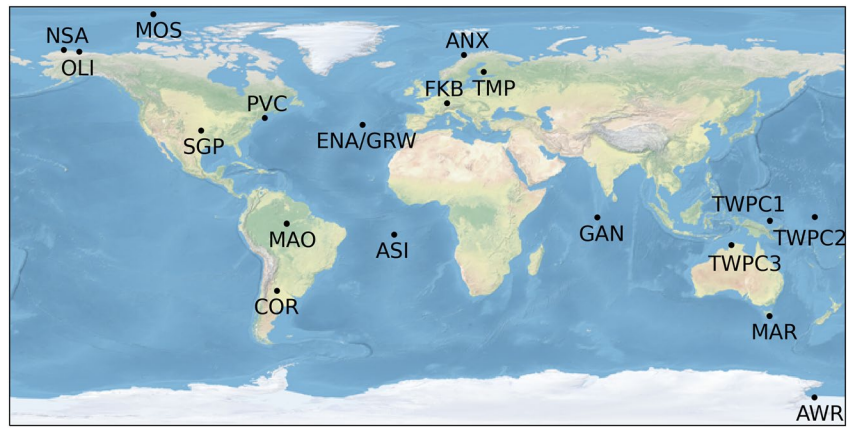

Figure 1. Map of all Atmospheric Radiation Measurement (ARM) sites considered. The location descriptions for each site are provided in Table 1.

ARM Tropical Western Pacific (TWP; Long et al., 2016) long-term sites (i.e., TWPC1, TWPC2, TWPC3) and Cordoba, Argentina (COR). The COR site was a part of the Cloud, Aerosol, and Complex Terrain Interactions (CACTI) field campaign (Varble et al., 2021). See Figure 1 for a map of the sites and Table 1 for the associated time period at each site.

The cloud boundaries from the ARSCL data product are also considered for sites where the CLDTYPE data product is not available. The site information for sites that consider the ARSCL data product is also provided in Figure 1 and Table 1. The ARSCL data product is considered from the KAZR and W-Band ARM Cloud Radar (WACR) where available. The analysis of the ARSCL data products is the same as that of the CLDTYPE data product except it only considers the cloud boundaries.

Table 1
The Site Abbreviation (Left), Location Description (Left Middle), and Time Periods (Right Middle) Considered and the Resulting Decorrelation Length Scale (in km) With 1-σ Errors From Figure 8 (Right)

Site abbreviation	Location	Time period	Decorrelation length scale (km)
SGP	Lamont, Oklahoma, United States	8 November 1996 to 29 September 2021	1.84 ± 0.01
COR	Cordoba, Argentina	23 September 2018 to 30 April 2019	2.03 ± 0.04
TWPC1	Manus, Papua New Guinea	1 July 1999 to 2 May 2014	2.05 ± 0.01
TWPC2	Nauru Island	1 November 1998 to 13 February 2009	1.77 ± 0.01
TWPC3	Darwin, Australia	1 January 2003 to 2 May 2014	2.29 ± 0.01
ANX	Andenes, Norway	1 December 2019 to 31 May 2020	1.38 ± 0.14
ASI	Ascension Island, South Atlantic	12 July 2016 to 30 September 2017	1.39 ± 0.06
AWR	McMurdo Station, Antarctica	18 November 2015 to 2 January 2017	1.12 ± 0.53
ENA	Azores, Eastern North Atlantic	17 July 2015 to 30 September 2021	1.67 ± 0.01
GRW	Azores, Eastern North Atlantic	6 June 2009 to 31 December 2010	1.80 ± 0.01
GAN	Gan Island, Maldives	9 October 2011 to 7 February 2012	1.43 ± 0.02
MOS	Ship in Arctic Ocean, MOSAiC Field Campaign	11 October 2019 to 1 October 2020	1.03 ± 0.15
NSA	North Slope of Alaska	11 November 2011 to 30 September 2021	1.24 ± 0.02
OLI	Oliktok Point, Alaska, United States	1 October 2015 to 15 June 2021	1.38 ± 0.01
TMP	Hyytiälä, Finland	1 February 2014 to 13 September 2014	1.18 ± 0.02
FKB	Black Forest, Germany	29 March 2007 to 1 January 2008	1.53 ± 0.01
MAO	Manacapuru, Brazil	18 February 2014 to 30 November 2015	3.06 ± 0.01
MAR	Ship in Southern Ocean, MARCUS field campaign	29 October 2017 to 24 March 2018	1.17 ± 0.02
PVC	Cape Cod, United States	12 October 2012 to 14 June 2013	1.89 ± 0.02

In addition to the CLDTYPE cloud classification, shallow cumulus identified time periods are also considered at the SGP site from the Shallow Cumulus (SHALLOWCUMULUS) VAP (Flynn et al., 2018). The SHALLOWCUMULUS data product utilizes the CLDTYPE data product as well as cloud occurrence and cloud fraction information from the ceilometer and the total sky imager to identify shallow cumulus time periods.

3. Cloud Vertical Overlap Characteristics From Observations Methods

The cloud observations are analyzed to derive cloud vertical overlap characteristics. We follow the methods described in Hogan and Illingworth (2000) as well as similar studies (e.g., Mace & Benson-Troth, 2002; Naud et al., 2008). The one exception in this present study is the upper limit considered for the layer cloud fraction (CF). Hogan and Illingworth (2000) consider partial cloudy layers where the layer CF (in both layers 1 and 2) is between 0 and 1 (i.e., $0 < CF_1, CF_2 < 1$), while only layer CFs up to 0.5 are considered in this study following recent studies to limit data truncation impacts on the results (e.g., Li et al., 2019; Tompkins & Di Giuseppe, 2015). The upper limit for the layer CF of 0.5 also excludes clouds associated with synoptic-scale and deep convective systems, which allows the analysis to focus on clouds that are more sensitive to the decorrelation length scale.

The cloud boundaries are converted into a cloud mask considering a temporal resolution of 1 hr and vertical resolution of 360 m. Profiles are only considered for nonprecipitating times when both the radar and lidar are available. In addition, only cloud boundaries that pass quality control tests are considered (i.e., qc flag = 0). If any profile in a 1 hr period do not meet these criteria, the cloud vertical overlap characteristics are not calculated.

For every 1 hr period, each pair of partial cloudy layers is considered (excluding comparing a layer to itself). The true CF (CF_{true}) is determined by considering the CF of the two layers combined. The maximum overlap (CF_{max}), minimum overlap (CF_{min}), and random overlap (CF_{rand}) CFs are calculated for each partial cloudy layer pair:

$$CF_{max} = \max(CF_1, CF_2) \tag{1}$$

$$CF_{min} = \min(1, CF_1 + CF_2) \tag{2}$$

$$CF_{rand} = CF_1 + CF_2 - CF_1 * CF_2 \tag{3}$$

where CF_1 and CF_2 are CFs in the two layers. The overlap parameter, α, is also calculated for each partial cloudy layer pair. The overlap parameter relates the CF_{true} to CF_{max} and CF_{rand}, such that:

$$CF_{true} = \alpha CF_{max} + (1 - \alpha) CF_{rand} \tag{4}$$

where when α equals 0, the overlap corresponds to random overlap and when α equals 1, the overlap corresponds to maximum overlap. When α is negative, the overlap corresponds to minimum overlap.

The vertical overlap characteristics are binned by vertical layer separation (i.e., $\Delta z = z_2 - z_1$). The analysis is further separated into two categories: (a) vertically continuous clouds, and (b) vertically noncontinuous clouds. Cloud layer pairs are considered vertically continuous clouds if every layer in-between the two layers compared are cloudy (i.e., CF > 0). Vertically noncontinuous cloud is considered if any layer is clear-sky in-between the two layers compared (i.e., CF = 0). For vertically continuous clouds, Hogan and Illingworth (2000) proposed an exponential relationship that relates α and Δz with a characteristic decorrelation length scale L_α:

$$\alpha = exp\left(-\frac{\Delta z}{L_\alpha}\right) \tag{5}$$

where the decorrelation length scale modulates the transition from maximum to random overlap with increasing layer separation. Observations of α and Δz are fit to Equation 5 to identify the decorrelation length scale that best fits observations. The fit of α and Δz to Equation 5 considers all cloud layer pairs in Sections 5.1.1 and 5.2 and for selected cloud type pairs in Sections 5.1.2, 5.1.3, and 5.2.1. Note that in general there are more samples at small layer separations and, therefore, the fit to Equation 5 is weighted toward smaller layer separations.

4. Decorrelation Length Scale Impact on the Surface Radiative Budget

To understand the implication of the decorrelation length scale on surface radiative fluxes, idealized layer CF and layer liquid water path (LWP) profiles are generated and considered (Figure 2a) as input into a radiative transfer

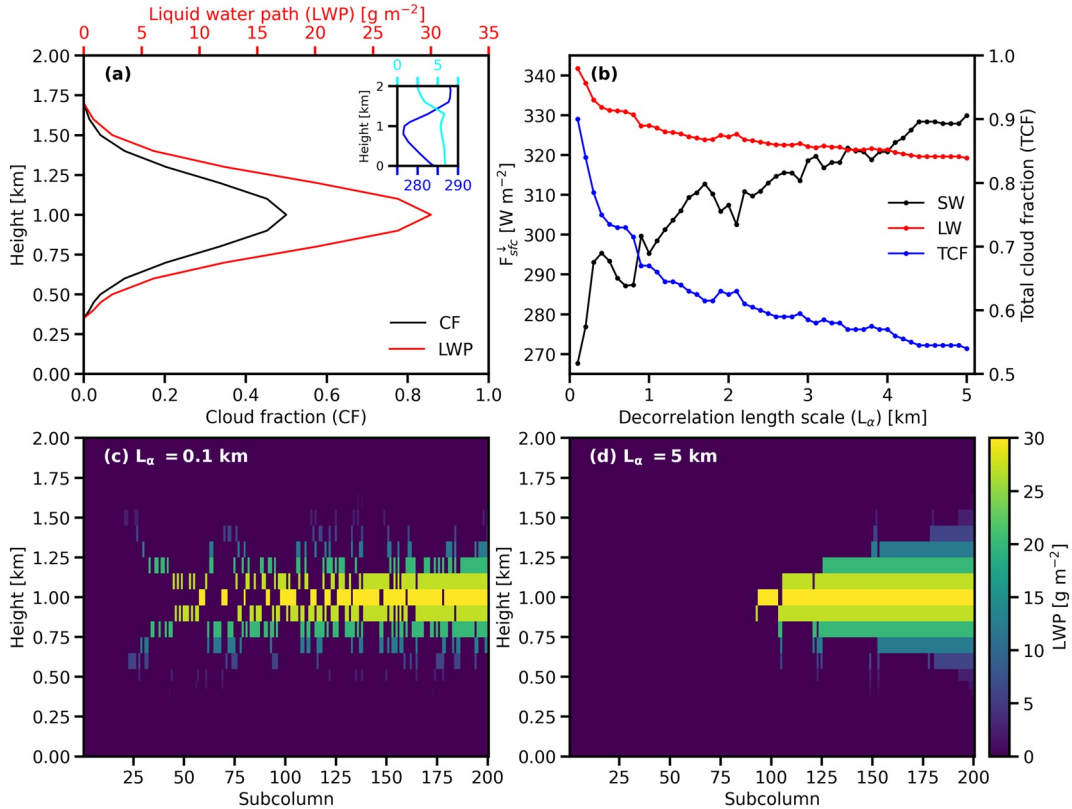

Figure 2. (a) Input cloud fraction (CF) and layer cloud liquid water path (LWP [g m^{-2}]) vertical profiles and (b) resultant surface downwelling fluxes ($F^{\downarrow}_{sfc}$ [W m^{-2}]) for shortwave (SW; black) and longwave (LW; red) and the total cloud fraction (TCF; blue) for the exponential-random cloud vertical overlap method with varying decorrelation length scale (L_α; km). Layer cloud LWP vertical profiles for each subcolumn ordered by increasing column LWP are shown for a decorrelation length scale of (c) 0.1 km, and (d) 5 km. (a) The temperature [K] (blue) and water vapor mixing ratio [g kg^{-1}] (light blue) profiles considered are shown in the inset.

model and the decorrelation length scale is varied. The layer CF profile considered has a maximum CF of 0.5 at 1 km and CFs greater than 0 from 0.4 to 1.6 km. The layer LWP profile considered is similar to the CF profile with a maximum layer LWP of 30 g m^{-2} at 1 km with layer LWPs greater than 0 from 0.4 to 1.6 km with a column LWP of 59.5 g m^{-2}. The idealized cloud profiles are generated to represent a low cloud situation with a column LWP typical at the SGP site.

Cloud fields are generated with the layer CF and layer LWP profiles following the exponential-random overlap method with decorrelation length scale values ranging from 0.1 to 5 km every 100 m considering 200 subcolumns. The stochastic cloud generator subroutine in Rapid Radiative Transfer Model for General Circulation Models (RRTMG) (Iacono et al., 2008) is utilized to generate the cloud fields considered here. Examples of the cloud fields for a decorrelation length scale of 0.1 and 5 km are shown in Figures 2c & 2d, respectively. The cloud fields are then input into the rapid radiative transfer model (RRTM) (Iacono et al., 2000; Mlawer et al., 1997). The radiative flux outputs are averaged following the Monte Carlo Independent Column Approximation (MCICA) (e.g., Pincus et al., 2003). Here the layer LWP profile is considered as input instead of the layer liquid water content (LWC) profile as the layer LWP is the input option considered for RRTM. Layer LWP is related to layer LWC by vertically integrating LWC across the depth of each layer.

In addition to the cloud field, other inputs considered in RRTM come from a high-resolution rapid refresh (HRRR) (Dowell et al., 2022) 1-hr forecast on 10 October 2019 initialized at 20 UTC at the SGP site. The solar zenith angle is 57.8°, which corresponds to an incoming top-of-atmosphere (TOA) solar flux of 732.3 W m^{-2}. The temperature and water vapor mixing ratio profiles are shown in the inset in Figure 2a.

The resultant surface SW and longwave (LW) downwelling fluxes are shown in Figure 2b. The surface SW downwelling fluxes (SW_{down}) range from 267.7 W m^{-2} for a decorrelation length scale of 0.1 km to 330.0 W m^{-2}

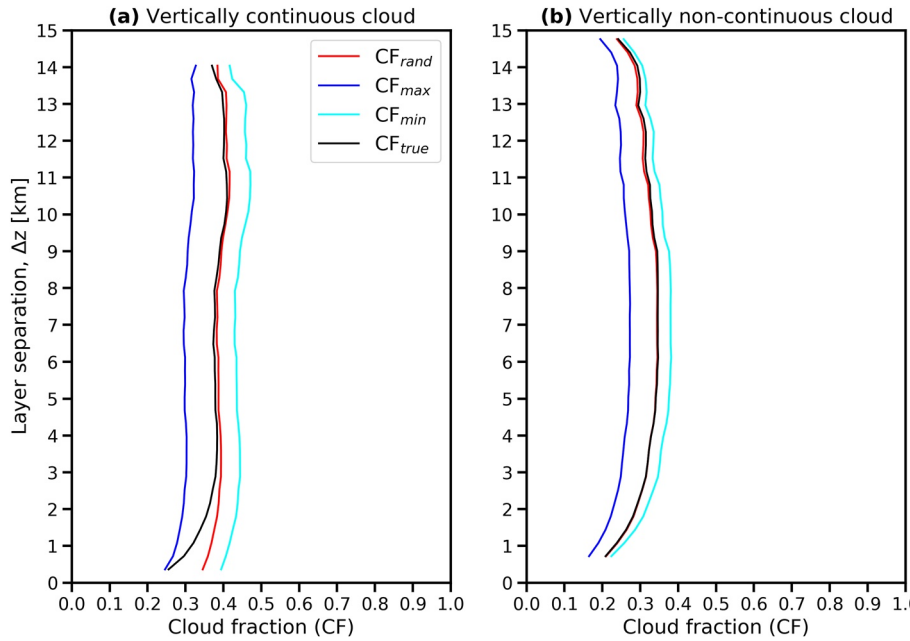

Figure 3. The mean cloud fractions (CF) for each layer separation (in km) for (a) vertically continuous clouds, and (b) vertically noncontinuous clouds at the Atmospheric Radiation Measurement Program Southern Great Plains site. The random (CF_{rand}; red), maximum (CF_{max}; dark blue), minimum (CF_{min}; light blue), and true (CF_{true}; black) cloud fractions are shown.

for a decorrelation length scale of 5 km. The SW_{down} increases with increasing decorrelation length scale due to the number of clear-sky subcolumns increasing as the overall cloud field moves more toward maximum overlap (e.g., Figure 2d compared to Figure 2c). The total CF (i.e., number of cloudy subcolumns divided by the total number of subcolumns) decreases from 0.90 to 0.54 when the decorrelation length scale changes from 0.1 to 5 km (Figure 2b). Nearly half of the 62.2 W m^{-2} change in SW_{down} occurs when the decorrelation length scale changes from 0.1 to 1 km (27.6 W m^{-2}) which corresponds to a decrease in the total CF of 0.90 to 0.67.

The surface LW downwelling fluxes (LW_{down}) range from 341.8 W m^{-2} for a decorrelation length scale of 0.1 km to 319.3 W m^{-2} for a decorrelation length scale of 5 km. The LW_{down} decreases with increasing decorrelation length scale for the same reason stated above for SW_{down} changes: a decrease in the total CF with increasing decorrelation length scale decreases LW_{down}. The relative change in LW_{down} for a decorrelation length scale of 0.1 to 1 km compared to the change from 0.1 to 5 km is even larger (63.8%) than for SW_{down} (44.3%). Overall, the changes in the surface radiative budget are on the order of ∼60 W m^{-2} for SW_{down} and ∼20 W m^{-2} in LW_{down} for the same CF and LWP profiles. This highlights the importance of investigating the observed decorrelation length scale, which is the focus of this study, in order to use correct overlap statistics in models.

5. Results

5.1. SGP Vertical Overlap Characteristics

The mean CF_{true}, CF_{max}, CF_{rand}, and CF_{min} for each layer separation are shown in Figure 3 for the SGP site. For vertically continuous clouds (Figure 3a), the CF_{true} is similar to CF_{max} at small layer separations before starting to transition closer to similar values as CF_{rand} as the layer separation increases beyond 360 m and reaching similar values as CF_{rand} near 4 km. For vertically noncontinuous clouds (Figure 3b), CF_{true} is similar to CF_{rand} for small and large layer separations. These results are comparable to other cloud vertical overlap studies based on observations at the SGP site (e.g., Li et al., 2019; Mace & Benson-Troth, 2002; Naud et al., 2008) as well as other cloud vertical overlap studies at other locations (e.g., Hogan & Illingworth, 2000).

The mean α binned by layer separation is shown in Figure 4 for the SGP site. For vertically continuous clouds (Figure 4a), the mean α is 0.91 for the smallest layer separation (i.e., 360 m). As the layer separation increases, mean α values decrease and approach values of ∼0.10 near 4 km. The mean α values align with the mean CF

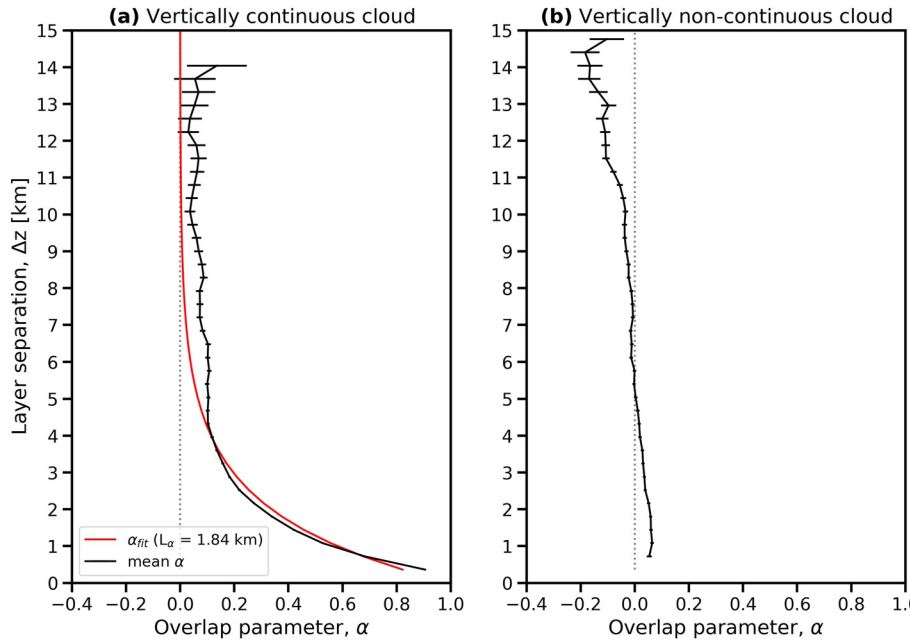

Figure 4. The mean overlap parameter (α) for each layer separation (in km) for (a) vertically continuous clouds, and (b) vertically noncontinuous clouds at the Atmospheric Radiation Measurement Program Southern Great Plains site (black). The exponential-random α values corresponding to Equation 5 with a decorrelation length scale of 1.84 km that fits the observations are shown in red. The standard error of the mean α is denoted by the black horizontal lines.

values (Figure 3a) such that α is near 1 (i.e., maximum overlap, $CF_{true} \sim CF_{max}$) at small layer separations and decreases toward 0 (i.e., random overlap, $CF_{true} \sim CF_{rand}$) at larger layer separations. For vertically noncontinuous clouds (Figure 4b), the mean α is 0.05 for the smallest layer separation (i.e., 720 m). Mean α values decrease slightly as layer separation increases with values near zero around 5 km. These mean α also align with the mean CF values (Figure 3b) as α is near 0 regardless of layer separation (i.e., random overlap, $CF_{true} \sim CF_{rand}$).

The α observations at the SGP site are fit to Equation 5 to obtain a decorrelation length scale. For the SGP site, the decorrelation length scale that fits the observations is 1.84 km. Mace and Benson-Troth (2002) found a decorrelation length scale of 3.94 km and Naud et al. (2008) found a decorrelation length scale of 1.4 km. While the values presented in this study are comparable to those of previous studies, the values are different. We attempt to compare our results to the previous results by considering our methodology but for layer CFs < 1 (instead of layer CFs < 0.5) and for the same time periods to better match the methods. For Naud et al. (2008), their time period considered is September 2002 to August 2004 for winter months only (i.e., November-March). Our decorrelation length scale is found to be 1.30 km for the Naud et al. (2008) time period and layer CF < 1, which is within 0.1 km of their value. For Mace and Benson-Troth (2002), their time period considered is March 1997 to December 2000 and our decorrelation length scale is found to be 1.88 km. In addition to different data products considered, Naud et al. (2008) found that their decorrelation length scale values differed from Mace and Benson-Troth (2002) due to differences in removal of precipitation times and cloud layer height maximum. This may explain the majority of the differences here as both effects would increase the decorrelation length scale. Overall, differences still exist between this study and the previous studies that preclude direct comparison due to differences in data products utilized and methodologies. In addition, the observations in this study benefit from improvements in the cloud radar systems (i.e., KAZR compared to the MMCR) as well as retrieval algorithm maturity (i.e., improved ARSCL, development of CLDTYPE).

The sensitivity of the decorrelation length scale to the CF threshold is assessed by considering various cloud layer CF thresholds. Previous studies considered cloud layer CFs less than 1 (e.g., Hogan & Illingworth, 2000). The decorrelation length scale at the SGP site that fits the observations when considering cloud layer CFs less than one is 1.50 km. Other CF thresholds tested include CF < 0.4 and CF < 0.6, which resulted in decorrelation length scales of 1.90 and 1.77 km, respectively. The decorrelation length scale decreases when increasing the CF threshold as more discontinuous clouds exhibiting minimum overlap appear in the analysis as noted in Tompkins

and Di Giuseppe (2015). The sensitivity of the decorrelation length scale to the vertical and temporal resolution is also considered. The decorrelation length scale for a vertical resolution of 100 and 500 m is 1.73 and 1.93 km, respectively. The decorrelation length scale for a temporal resolution of 30 min and 2 hr is 1.98 and 1.76 km, respectively. Except for considering a CF < 1, the sensitivity of the decorrelation length scale to the methods is within ∼0.10–0.15 km, which corresponds to differences on the order of a few W m^{-2} in the SW_{down} (Figure 2b).

The α observations at the SGP site are separated by season and fit to Equation 5 to obtain a seasonal decorrelation length scale. The decorrelation length scale that fits the seasonal observations are: 1.57 km for winter (December–February; DJF), 1.72 km for spring (March–May; MAM), 2.16 km for summer (June–August; JJA), and 1.90 km for fall (September–November; SON). The seasonal cycle of the decorrelation length scale at the SGP site is such that the decorrelation length scale value is largest in the summer and smallest in the winter, which has also been noted in Mace and Benson-Troth (2002), Oreopoulos and Norris (2011), and Li et al. (2019). Li et al. (2019) suggests that the decorrelation length scale seasonal cycle is due to the relative strength of the wind shear and instability. Weaker wind shear and a more unstable atmosphere correspond to maximum cloud vertical overlap and therefore a larger decorrelation length scale is observed in the summer compared to the winter. The seasonal cycle of the mean α at various layer separations (i.e., 1, 2, 4, and 6 km) are compared to those in Mace and Benson-Troth (2002) (see their Figure 7) (not shown). The seasonal cycle is similar to those in Mace and Benson-Troth (2002), except that the mean α for a given season and layer separation is smaller in magnitude in this study, likely due to the differences between the studies mentioned above.

5.1.1. SGP Decorrelation Length Scales by Cloud Types

The previous section considered vertical overlap observations regardless of cloud type. In this section, α values are separated by cloud type classification for vertically continuous clouds. The methods are the same as described in Section 3 with additional information for the cloud type classification that is matched to the cloud mask and identified for each cloud layer separately based on Lim et al. (2019). Within a temporal resolution of 1 hr, the cloud type classification in a given layer can be one (e.g., cirrus) or more than one (e.g., cirrostratus/anvil and cirrus). The two cloud layers are analyzed for their overlap properties and then categorized into the associated cloud type pair classification (e.g., cirrostratus/anvil and cirrus paired with cirrus). Each cloud layer pair is analyzed and then aggregated by cloud type pairs. Note that other cloud types may exist in-between the two layers analyzed since the analysis is restricted to vertically continuous clouds. In addition, the layer CF threshold of 0.5 limits the cloud type analyzed as frequent cloud type pairs. For example, deep convection clouds often do not meet this criterion and, therefore, are not included in a frequent cloud type pair.

The mean α for each layer separation for the 10 most frequent cloud type pairs are shown in Figure 5. The decorrelation length scale for each cloud type pair is also found following Equation 5. The number of samples for the 10 most frequent cloud type pairs are provided in Table 2. Overall, the mean α values show similarities but also distinct differences across different cloud type pairs. The most frequent cloud type pair is cirrus paired with cirrus, which has a decorrelation length scale of 1.36 km. The mean α at the smallest layer separation for cirrus paired to cirrus has a similar value (0.90) as that regardless of cloud type (0.91). This is the case for other cloud type pairs as well, for example, cirrostratus/anvil and cirrus paired with cirrostratus/anvil and cirrus. The mean α for cirrus paired with cirrus decreases toward 0 (i.e., random overlap) at smaller layer separations than when observations are considered regardless of cloud type, which is further indicated by a decorrelation length scale that is smaller than that without regard for cloud type (1.84 km, Figure 4a). The decorrelation length scale value for cirrus paired with cirrus may be smaller than other cloud type pairs due to subsidence at upper levels or large wind shear (Naud et al., 2008).

The smallest decorrelation length scale by cloud type pair is 0.04 km for cirrostratus/anvil paired with cirrus. The small value indicates that the overlap observations for this cloud type pair are closer to random overlap than to maximum overlap, even at small layer separations. This is further seen in that the mean α at a layer separation of 360 m is 0 and decreases to around −0.15 for larger layer separations. The negative α values indicate that the cloud type pair correspond to minimum overlap for layer separations of 720 m and greater. The negative α values are not represented by the decorrelation length scale since Equation 5 cannot represent negative values. Therefore, the decorrelation length scale is near 0 as a consequence. The minimum overlap observed for the cirrostratus/anvil paired with cirrus may be due to large vertical shear of the horizontal wind, which favors minimum overlap (Naud et al., 2008).

The largest decorrelation length scale by cloud type pair is 4.58 km for low cloud paired with cirrus. The mean α values are centered around 0.2 with layer separations only greater than 3 km. The large layer separations

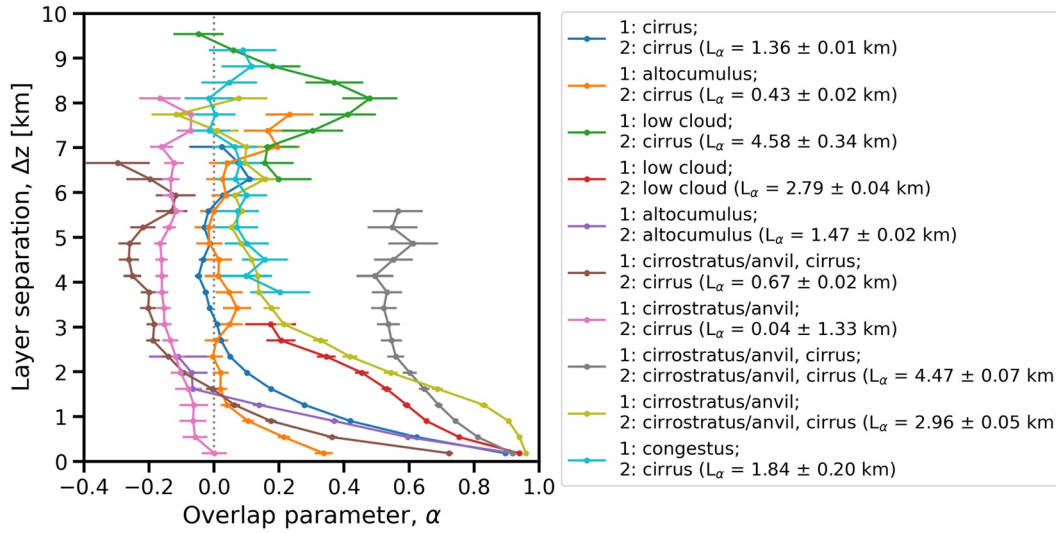

Figure 5. The mean overlap parameter (α) for each layer separation (Δz; km) for vertically continuous clouds at the Atmospheric Radiation Measurement Program Southern Great Plains site. The observations are separated by cloud types with the most frequent cloud regimes shown. The cloud types for each regime are given for the lower (1) and upper cloud layers (2). The decorrelation length scale (km) and the 1-σ error for each cloud regime is given in the parentheses. The standard error of the mean α is denoted by the horizontal lines.

Table 2
The Number of Samples for the 10 Most Frequent Cloud Type Pairs (Top Right) and the Cloud Height Classification Pairs (Bottom Right)

Cloud type		
Lower cloud layer	Upper cloud layer	Number of samples
Cirrus	Cirrus	222,020
Altocumulus	Cirrus	34,841
Low cloud	Cirrus	28,692
Low cloud	Low cloud	22,547
Altocumulus	Altocumulus	15,436
Cirrostratus/anvil, cirrus	Cirrus	14,294
Cirrostratus/anvil	Cirrus	12,688
Cirrostratus/anvil, cirrus	Cirrostratus/anvil, cirrus	11,426
Cirrostratus/anvil	Cirrostratus/anvil, cirrus	11,087
Congestus	Cirrus	7,910
Cloud height classification		
Lower cloud layer	Upper cloud layer	Number of samples
High-level cloud	High-level cloud	271,288
Mid-level cloud	High-level cloud	104,987
Low-level cloud	High-level cloud	79,123
Low-level cloud	Low-level cloud	54,263
Low-level cloud	Mid-level cloud	46,271
Mid-level cloud	Mid-level cloud	37,867

Note. The cloud types and cloud height classification for each regime are given for the lower (left) and upper cloud layers (middle).

for low cloud paired with cirrus are the result of the cloud type classification thresholds as low clouds are only classified at heights below 3.5 km and cirrus are only defined at heights above 6.5 km (see Table 1 in Lim et al. (2019)). The low cloud paired with cirrus mean α values are less than 0.5 for all layer separations considered, which suggests that the cloud type pair is closer to random overlap than to maximum overlap. Despite the small α values, the decorrelation length scale is large due to the large layer separations as the result of comparing the low and high clouds. Consequently, the decorrelation length scale and Equation 5 do not represent the α values well, which was also the case for the cirrostratus/anvil paired with cirrus cloud type pair. While the low cloud paired with cirrus mean α values are always less than 0.5, the mean α values are greater than 0.2 for layer separations from ~6 to ~9 km. These values are also larger than other cloud type pairs (e.g., congestus paired with cirrus) that have mean α values closer to 0 for similarly large layer separations. This suggests that overlap is not always random at large layer separations (e.g., 8 km) for vertically continuous clouds as often assumed within models.

Of the 10 most frequent cloud type pairs, 8 cloud type pairs are comprised of cirrus clouds in either the lower or upper cloud layer considered. In addition, half (4) of the cirrus cloud type pairs are combinations of cirrus and cirrostratus/anvil, for example, cirrostratus/anvil paired with cirrus cloud type pair. Despite similarities in cloud type classification, the decorrelation length scale ranges from 0.04 km for cirrostratus/anvil paired with cirrus to 4.47 km for cirrostratus/anvil and cirrus paired with cirrostratus/anvil and cirrus. The large spread in the decorrelation length scale among the cirrus and cirrostratus/anvil combinations separate into two groups according to if cirrostratus/anvil is present in the upper cloud layer considered or not. If only cirrus clouds are in the upper cloud layer, the decorrelation length scale is small (0.04 or 0.67 km). In contrast, if cirrostratus/anvil is present in the upper cloud layer considered, the decorrelation length scale is larger (2.96 or 4.47 km).

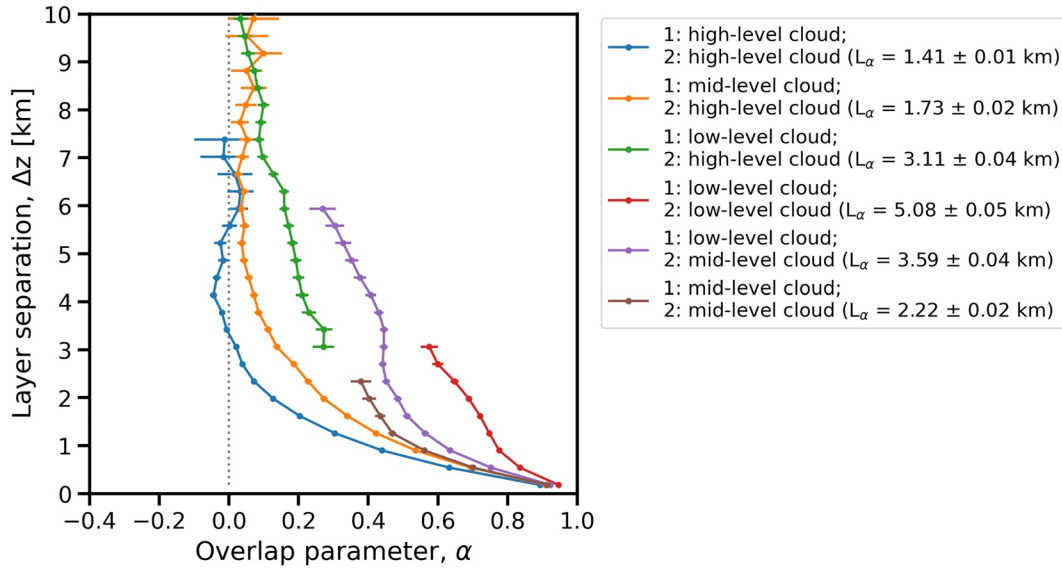

Figure 6. The mean overlap parameter (α) for each layer separation (Δz; km) for vertically continuous clouds at the Atmospheric Radiation Measurement Program Southern Great Plains site separated by cloud layer height into low-level, mid-level, and high-level clouds. The cloud layer height classifications are given for the lower (1) and upper cloud layers (2). The decorrelation length scale (km) and the 1-σ error for each cloud layer height classification pair is given in the parentheses. The standard error of the mean α is denoted by the horizontal lines.

We also consider the decorrelation length scale for cloud type pairs that are comprised of a single cloud type, for example, low cloud paired with low cloud. Several single cloud type pairs are already found in Figure 5 as part of the top 10 most frequent cloud type pairs. In addition to those in Figure 5, congestus, deep convection, altostratus, and cirrostratus/anvil single cloud type pairs are investigated and found to have decorrelation length scales of 9.22, 18.09, 2.66, and 3.95 km, respectively. Similar to all cloud type pairs, cirrus paired with cirrus has the smallest decorrelation length scale. The largest decorrelation length scale is deep convection paired with deep convection as expected due to their association with atmospheric instability that supports vertical growth and ultimately maximum overlap.

5.1.2. SGP Decorrelation Length Scales by Cloud Layer Height Classification

The α and decorrelation length scale values are also separated into cloud layer height classification. The cloud layers are classified as low-level (height <3.5 km), mid-level (3.5 km < height < 6.5 km), or high-level clouds (height > 6.5 km), which is based on the cloud type classification criteria used in Lim et al. (2019) (see their Table 1). The mean α for each layer separation for the cloud layer height classification pairs are shown in Figure 6. The decorrelation length scale for each cloud layer height classification pair is also found following Equation 5. The number of samples for the cloud layer height classification pairs are provided in Table 2.

Similar to Figures 4 and 5, the mean α values are near 0.90 for the smallest layer separation of 360 m for nearly all cloud layer height classifications in Figure 6. The only exception is the low-level cloud paired with high-level cloud pair in which the smallest layer separation is 3 km. The high-level paired with high-level cloud pair is the most frequent cloud layer height classification and also decreases toward mean α values of 0 at smaller layer separations than compared to other cloud layer height classification pairs. This is also noted in the high-level paired with high-level cloud pair decorrelation length scale, which is 1.41 km and the smallest decorrelation length scale value when considering height classification. The high-level paired with high-level cloud pair decorrelation length scale value is similar to that for cirrus paired with cirrus. This is due to the height classification criteria being based on the cloud type classification and, therefore, a large overlap in samples between cirrus paired with cirrus and high-level paired with high-level.

The largest decorrelation length scale by cloud height classification is 5.08 km for low-level cloud paired with low-level cloud. The decorrelation length scale value is considerably larger than the low cloud paired with low cloud value in Section 5.1.1, which is due to other cloud type classifications being considered when only

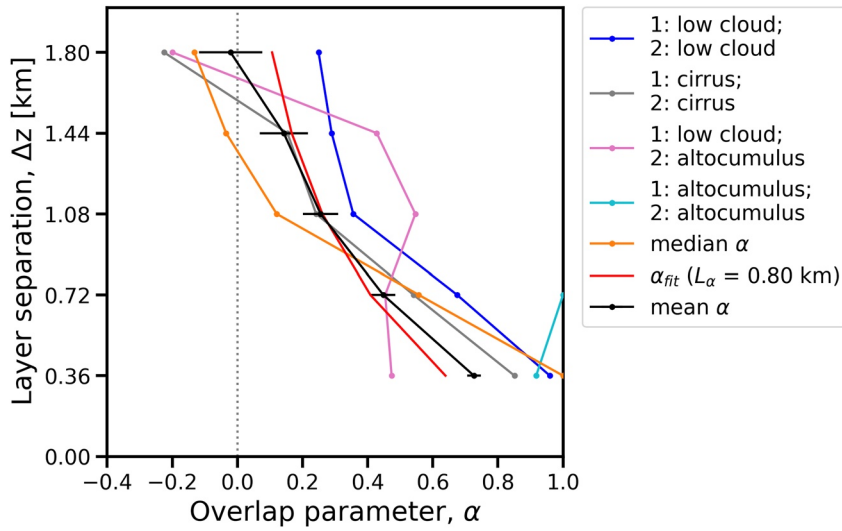

Figure 7. The mean (black) and median (orange) overlap parameter (α) for each layer separation (Δz; km) for vertically continuous clouds during identified shallow cumulus times at the ARM SGP site. The mean α observations separated by cloud types are also shown. The cloud types for each regime are given for the lower (1) and upper cloud layers (2). The α values corresponding to a decorrelation length scale of 0.80 km that is based on fitting the mean α observations to Equation 5 are shown in red. The standard error of the mean α is denoted by the black horizontal lines.

considering cloud height classification. For example, congestus and deep convection cloud types are included when considering low-level clouds as cloud heights below 3.5 km. These cloud types are often associated with atmospheric instability favoring vertical motion that tend to be more maximally vertically overlapped (Li et al., 2019) compared to other cloud types, therefore, increasing the decorrelation length scale. The decorrelation length scale value for the low-level cloud paired with low-level cloud may be larger than the high-level cloud paired with high-level cloud as a result of this as well as stronger upper-level horizontal winds that may spread out the cloud horizontally rather than vertically.

5.1.3. SGP Shallow Cumulus Decorrelation Length Scales

Cloud vertical overlap observations are also considered for periods of shallow cumulus clouds. The shallow cumulus time periods are from the SHALLOWCUMULUS data product (Section 2). While the focus is on the occurrence of shallow cumulus clouds (i.e., low clouds) during these time periods, other cloud types that occur are also considered, which include cirrus and altocumulus. The methods applied are the same as those in Section 3 except the 1 hr periods considered are centered on the hour mark to follow the SHALLOWCUMULUS data product time bounds considered, for example, 0:30 to 1:30. The other analysis presented start at the hour mark, for example, 0:00 to 1:00.

The mean α for each layer separation for clouds during shallow cumulus identified times are shown in Figure 7. The decorrelation length scale considering shallow cumulus identified times is also found following Equation 5 by considering the mean α values. The resultant decorrelation length scale is 0.80 ± 0.09 km, which is considerably smaller than that considering all clouds (i.e., 1.84 km; Figure 4). The median α at a layer separation of 360 m is 1, which indicates that a majority of the clouds analyzed are maximally overlapped. The mean α at a layer separation of 360 m is 0.73, which indicates that the minority of clouds that diverge from maximum overlap have smaller α values closer to random overlap instead of α values near 1 and maximum overlap. This is further seen in the 25th percentile, which is 0.57 at a layer separation of 360 m. At layer separations of 1 km and greater, the mean α is greater than the median α. This suggests the opposite seen for layer separations below 1 km such that the majority of clouds analyzed have an α near 0 corresponding to random overlap, while the minority tend toward maximum overlap. This is further supported by the 75th percentile, which is 1.0 at a layer separation of 1.08 km.

The cloud type classifications are also considered for the shallow cumulus time periods and shown in Figure 7. At the smallest and largest layer separations, low cloud paired with low cloud have the largest mean α values. Low

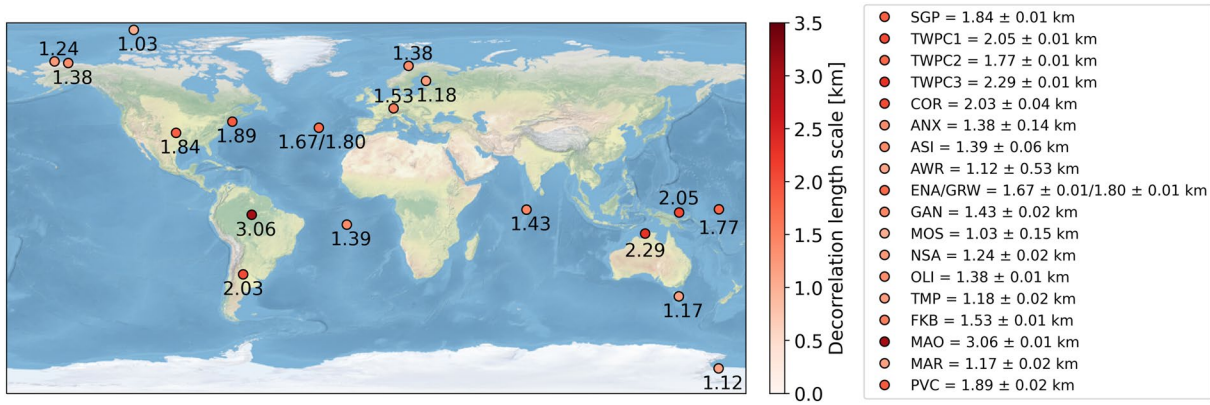

Figure 8. A map of the decorrelation length scale (km) that fits observations at all Atmospheric Radiation Measurement Program (ARM) sites considered. Lighter shades of red correspond to smaller decorrelation length scales and darker shades correspond to larger decorrelation scales. The values are labeled next to each site's latitude and longitude as well as in the legend (with 1-σ errors) and included in Table 1.

cloud paired with altocumulus have the largest mean α value at medium layer separations (e.g., 1.08 km), which is in contrast to smaller and larger layer separations when the low cloud paired with altocumulus mean α values are typically smaller than other regimes. In general, cirrus paired with cirrus mean α values are smaller compared to the other cloud type pairs. This indicates the values are closer to random overlap than other cloud type pairs, which is also seen in Figure 5 when considering all times instead of shallow cumulus periods only. The largest mean α values for a cloud type pair are from the altocumulus paired with altocumulus cloud type pair, which is 0.92 and 1.0 at layer separations of 360 and 720 m. The large α values indicate altocumulus paired with altocumulus correspond well to maximum overlap. There are no continuous cloud layer pairs considered for altocumulus paired with altocumulus for layer separation of 1 km and greater, which is partially due to the fact that the cloud thickness of altocumulus is defined as less than 1.5 km in Lim et al. (2019).

The observationally derived decorrelation length scale in this study is larger than other studies that analyzed shallow cumulus from Large-Eddy Simulations (LES). For example, Neggers et al. (2011) found the shallow cumulus decorrelation length scale to be 200–300 m. We have also investigated applying our cloud vertical overlap methods to LES output for LES ARM Symbiotic Simulation and Observation (LASSO) cases (Gustafson et al., 2020) with shallow cumulus clouds. The LASSO case considered here is the 22 May 2018 case, which included shallow cumulus clouds and a maximum cloud top height of 4.275 km. The decorrelation length scale value is found to be 0.54 km. Our initial analysis also suggests that the decorrelation length scale is smaller for LES than those presented here based on shallow cumulus observations. It is our future research goal to investigate these differences further, including more cases that sample other shallow cumulus cases modeled.

5.2. Global Decorrelation Length Scales

The previous sections focused on results from the SGP site. In this section, the methodology is expanded to other long-term and short-term ARM sites where the CLDTYPE and ARSCL data product is available. The cloud vertical overlap characteristics are again calculated from observations of cloud vertical profiles and separated by cloud type where available.

The decorrelation length scale is found by fitting the α observations to Equation 5 for each site. A map with the decorrelation length scale value for each site is shown in Figure 8. The decorrelation length scale values for each site are also provided in Table 1. The smallest decorrelation length scale is 1.03 km in the Arctic as part of the Multidisciplinary Drifting Observatory for the Study of Arctic Climate (MOSAiC) field campaign (Shupe et al., 2022). The largest decorrelation length scale is 3.06 km in Manacapuru, Brazil as part of the Green Ocean Amazon (GoAmazon) field campaign (Martin et al., 2017).

The decorrelation length scale values are generally larger near the equator and decrease poleward in Figure 8, which has been noted previously (e.g., Oreopoulos et al., 2012; Shonk et al., 2010). However, this is not exhibited at all sites in Figure 8. For example, the decorrelation length scale at Ascension Island (ASI) in the South Atlantic

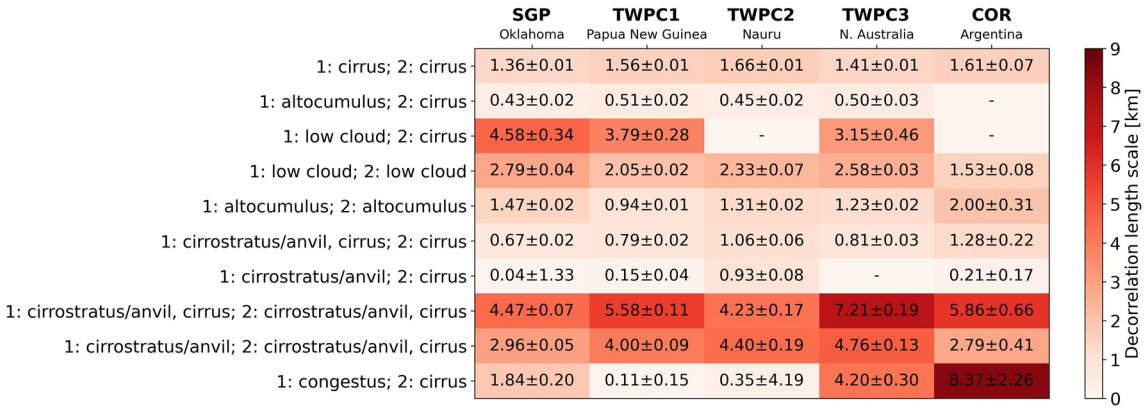

Figure 9. A chart of the decorrelation length scale (km) that fits observations by site (columns) and by cloud regime (rows) with 1-σ errors also shown. The sites include the SGP (left), TWPC1 (second from left), TWPC2 (middle), TWPC3 (second from right), and Cordoba, Argentina (COR) (right) sites. The cloud types for each regime are given for the lower (1) and upper cloud layers (2) to the left of the chart. Lighter shades of red correspond to smaller decorrelation length scales and darker shades correspond to larger decorrelation scales. Decorrelation length scale values for cloud regimes at sites with large errors are not shown and instead denoted with a dash.

Ocean and Gan Island (GAN) in the Maldives are 1.39 and 1.43 km, respectively, despite a similar latitude to the site in Manacapuru, Brazil (MAO) where the decorrelation length scale is twice in magnitude. The differences between ASI and GAN compared to MAO may be related to ocean-based sites compared to land-based sites. This difference has been noted in a global satellite-based study by Li et al. (2015), where they found that larger overlap values were found for land-based locations than for ocean-based locations. The larger overlap values for land-based compared to ocean-based may be due to typically larger land surface fluxes (Li et al., 2015), which may enhance instability and lead to increased vertical motion and hence increased vertical alignment over land as compared to over ocean. Besides MAO and TWPC3 in Darwin, Australia for 1 July to 1 January, the decorrelation length scale values for the tropical sites are smaller than those in Oreopoulos et al. (2012) by more than 1 km. The parameterization in Oreopoulos et al. (2012) is closer to the values in Figure 8 for the midlatitude and high-latitudes sites with all other sites within 0.5 km. However, the minimum value in the latitude-dependent decorrelation length scale parameterization in Oreopoulos et al. (2012) is 1.43 km, which is larger than half of the sites examined in this study. The decorrelation length scale values in Figure 8 are also compared to the absolute latitude parameterization in Shonk et al. (2010). In general, the decorrelation length scale in Figure 8 exhibited a smaller change with latitude. The midlatitude sites compare well but tropical sites are smaller and high-latitude sites are larger than the Shonk et al. (2010) parameterization. Similar to the comparison with Oreopoulos et al. (2012), the decorrelation length scale values agree within ~0.5 km besides several of the tropical sites including the TWP sites and the GAN site.

5.2.1. Global Decorrelation Length Scales by Cloud Types

In Section 5.1.1, the decorrelation length scale by cloud regime is shown for the SGP site. In this section, we find the decorrelation length scale for the same cloud regimes at other sites where the CLDTYPE data product is available, which includes the TWPC1, TWPC2, TWPC3, and COR sites. The decorrelation length scale values by cloud regime for each site considered are shown in Figure 9.

The cloud regimes correspond to those that were most frequent at the SGP site; however, the most frequent cloud regimes are different at each site due to differences in each location's cloud climatologies. We consider the same as those at the SGP site in order to compare and contrast how the decorrelation length scale changes across sites for the same cloud regimes.

There are several similarities in the decorrelation length scale value for a given cloud regime across the five different sites. For example, the decorrelation length scale values for the cirrus paired with cirrus cloud regime only ranges from 1.36 km at the SGP site in the continental midlatitudes to 1.66 km at the TWPC2 site located on an island near the equator. The similarities in the decorrelation length scale across different sites for the same cloud regime indicates that cloud regime information could help inform the decorrelation length scale to use within models that specify a decorrelation length scale.

In contrast, several cloud regimes show distinct differences including the congestus paired with cirrus cloud type pair. The decorrelation length scale value is greater than 1 km for the SGP, TWPC3, and COR sites, while the values are 0.1–0.4 km for the TWPC1 and TWPC2 sites. The former values indicate a larger layer separation before the transition to random overlap, while the latter suggest a transition to random overlap at only a couple hundred meters. The differences could be related to synoptic forcings playing a role as the formation of congestus and the formation of cirrus vary from site to site. Another possible difference could be due to the decorrelation length scale methodology not capturing the variation of α with layer separation for cloud type pairs that often have large layer separation, for example, congestus paired with high cloud. While the similarities in Figure 9 are encouraging, the differences in the decorrelation length scale across difference sites for the same cloud regime recommends caution should be used when considering global application of regime-specific decorrelation length scales for several of the cloud regimes.

6. Summary

Cloud vertical overlap characteristics are derived at the ARM SGP site from nearly 25 years of ground-based observations. Cloud vertical overlap characteristics are also derived from observations at other long-term ARM deployments including the TWP, North Slope of Alaska, and Eastern North Atlantic sites as well as other short-term field deployments across the globe. The cloud vertical overlap characteristics are derived from vertical profiles of clouds from the CLDTYPE and ARCL data products, which utilize radar and lidar observations from the MMCR, KAZR, WACR, and MPL.

The cloud vertical overlap observations are utilized to derive the decorrelation length scale. At the SGP site, the decorrelation length scale that fits observations is 1.84 km. Globally, the decorrelation length scale value ranged from 1.03 km in the Arctic to 3.06 km in Brazil.

The decorrelation length scale is also considered by cloud type classification. At the SGP site, the cloud type classified decorrelation length scale ranged from 0.04 km for cirrostratus paired with cirrus to 4.58 km for low cloud paired with cirrus. The decorrelation length scale is derived for shallow cumulus periods, which is found to be 0.80 km. The observationally derived decorrelation length scale presented in this study is larger than values from LES models suggest (on the order of a few 100s of meters). The discrepancy between observationally derived and LES-derived shallow cumulus decorrelation length scale is a finding we intend to investigate further in future research. The decorrelation length scale is also considered by height level classification at the SGP site. The decorrelation length scale value ranged from 1.41 km for high-level paired with high-level cloud pair to 5.08 km for low-level paired with low-level cloud pair.

The decorrelation length scale by cloud type classification is considered for other sites to assess how it varies by location for the same cloud regimes. The decorrelation length scale by cloud regime exhibited similarities (e.g., cirrus paired with cirrus) and differences (e.g., congestus paired with cirrus) when considering different locations globally. The similarities among cloud regime-specific cloud vertical overlap characteristics despite different climatologies and specifically cloud climatologies is encouraging that cloud regime can help inform decorrelation length scales when developing operational forecast models. However, the differences call for caution for several cloud regimes in which more information (e.g., wind shear and atmospheric stability) may be necessary to determine the decorrelation length scale and ultimately model a representative cloud-radiation interaction.

This study investigates how cloud vertical overlap observations varied by site, season, and cloud regime to inform model assumptions of subgrid-scale clouds. To understand how to implement these results, testing within a numerical weather prediction model set up could help identify the forecast utility. One way to investigate this is to adjust the cloud vertical overlap inputs and evaluate the modeled values against observations, such as with the surface radiative fluxes at the ARM sites included in this study. In addition to testing, several factors would need to be addressed. First, the applicability of the observed cloud type decorrelation length scale requires identifying comparable cloud types between the model and observations. In addition, the variability in the decorrelation length scale by cloud type could be implemented into a numerical model with a reliable cloud type diagnostic. The cloud height classification decorrelation length scale results could provide additional information to the model assumptions for subgrid-scale clouds that could avoid cloud type classification differences between observations and models.

Long-term ground-based observations from point-locations provide the opportunity to derive cloud vertical overlap characteristics and test cloud vertical overlap assumptions. Cloud vertical overlap assumptions are utilized by numerical weather prediction models to represent subgrid-scale clouds. This study derives cloud vertical overlap characteristics for all clouds and by cloud regimes that could potentially be implemented into numerical weather prediction models. By improving the representation of subgrid-scale clouds and their interaction with radiation within operational models, this could potentially improve prediction of radiative fluxes for weather, climate, and renewable energy forecasting.

Data Availability Statement

Data can be downloaded from the ARM data archive for the CLDTYPE (http://dx.doi.org/10.5439/1349884), KAZR ARSCL (http://dx.doi.org/10.5439/1393437), WACR ARSCL (http://dx.doi.org/10.5439/1097547), and SHALLOWCUMULUS (http://dx.doi.org/10.5439/1392569) VAPs.

Acknowledgments
The authors thank J. J. Gristey for providing LES output. This project was jointly supported by the National Oceanic and Atmospheric Administration (NOAA), Weather Portfolio Office (WPO), and NOAA Climate Portfolio Office (CPO). This work was partially supported by the NOAA Atmospheric Science for Renewable Energy (ASRE) program. This research was supported in part by NOAA Cooperative Agreements NA17OAR4320101 and NA22OAR4320151.

References

Ackerman, T. P., & Stokes, G. M. (2003). The atmospheric radiation measurement Program. *Physics Today*, *56*(1), 38–44. https://doi.org/10.1063/1.1554135

Atmospheric Radiation Measurement (ARM) User Facility. (2000). Fair-Weather Shallow Cumulus Identification (SHALLOWCUMULUS) [Dataset]. 2000-07-02 to 2021-09-29, Southern Great Plains (SGP) Central Facility, Lamont, OK (C1). Compiled by Y. Shi. ARM Data Center. https://doi.org/10.5439/1392569

Atmospheric Radiation Measurement (ARM) User Facility. (2016). W-band Cloud Radar Active Remote Sensing of Cloud (ARSCLWACR1KOLLIAS) [Dataset]. Compiled by S. Giangrande, K. Johnson, E. Clothiaux and P. Kollias. ARM Data Center. https://doi.org/10.5439/1097547

Atmospheric Radiation Measurement (ARM) User Facility. (2018). Cloud Type Classification (CLDTYPE) [Dataset]. Compiled by D. Zhang and Y. Shi. ARM Data Center. https://doi.org/10.5439/1349884

Atmospheric Radiation Measurement (ARM) User Facility. (2019). Active Remote Sensing of CLouds (ARSCL) product using Ka-band ARM Zenith Radars (ARSCLKAZR1KOLLIAS) [Dataset]. Compiled by K. Johnson, S. Giangrande and T. Toto. ARM Data Center. https://doi.org/10.5439/1393437

Chen, T., Zhang, Y., & Rossow, W. B. (2000). Sensitivity of atmospheric radiative heating rate profiles to variations of cloud layer overlap. *Journal of Climate*, *13*(16), 2941–2959. https://doi.org/10.1175/1520-0442(2000)013<2941:SOARHR>2.0.CO;2

Chou, M. D., Suarez, M. J., Ho, C. H., Yan, M. M. H., & Lee, K. T. (1998). Parameterizations for cloud overlapping and shortwave single-scattering properties for use in general circulation and cloud ensemble models. *Journal of Climate*, *11*(2), 202–214. https://doi.org/10.1175/1520-0442(1998)011<0202:PFCOAS>2.0.CO;2

Clothiaux, E. E., Miller, M. A., Turner, D. D., Mace, G. G., Marchand, R. T., Widener, K. B., et al. (2001). The ARM millimeter wave cloud radars (MMCRs) and the active Remote sensing of clouds (ARSCL) value added product (VAP). Retrieved from https://www.arm.gov/publications/tech_reports/arm-vap-002-1.pdf

Dowell, D. C., Alexander, C. R., James, E. P., Weygandt, S. S., Benjamin, S. G., Manikin, G. S., et al. (2022). The high-resolution rapid refresh (HRRR): An hourly updating convection-allowing forecast model. Part I: Motivation and system description. *Weather and Forecasting*, *37*(8), 1371–1395. https://doi.org/10.1175/WAF-D-21-0151.1

Flynn, D., Shi, Y., Lim, K.-S., & Riihimaki, L. (2017). Cloud type classification (CLDTYPE) value-added product. Retrieved from https://www.arm.gov/publications/tech_reports/doe-sc-arm-tr-200.pdf

Flynn, D., Shi, Y., Lim, K.-S., & Riihimaki, L. (2018). Shallow cumulus (SHALLOWCUMULUS) value-added product report. Retrieved from https://www.arm.gov/publications/tech_reports/doe-sc-arm-tr-214.pdf

Geleyn, J. F., & Hollingsworth, A. (1979). An economical analytical method for the computation of the interaction between scattering and line absorption of radiation. *Contributions to Atmospheric Physics*, *52*, 1–16.

Gustafson, W. I., Vogelmann, A. M., Li, Z., Cheng, X., Dumas, K. K., Endo, S., et al. (2020). The large-eddy Simulation (LES) atmospheric radiation measurement (ARM) Symbiotic Simulation and observation (LASSO) activity for continental shallow convection. *Bulletin of the American Meteorological Society*, *101*(4), E462–E479. https://doi.org/10.1175/BAMS-D-19-0065.1

Hogan, R. J., & Illingworth, A. J. (2000). Deriving cloud overlap statistics from radar. *Quarterly Journal of the Royal Meteorological Society*, *126*(569), 2903–2909. https://doi.org/10.1002/QJ.49712656914

Iacono, M. J., Delamere, J. S., Mlawer, E. J., Shephard, M. W., Clough, S. A., & Collins, W. D. (2008). Radiative forcing by long-lived greenhouse gases: Calculations with the AER radiative transfer models. *Journal of Geophysical Research*, *113*, D13103. https://doi.org/10.1029/2008JD009944

Iacono, M. J., Mlawer, E. J., Clough, S. A., & Morcrette, J. J. (2000). Impact of an improved longwave radiation model, RRTM, on the energy budget and thermodynamic properties of the NCAR community climate model, CCM3. *Journal of Geophysical Research*, *105*(D11), 14873–14890. https://doi.org/10.1029/2000JD900091

Kollias, P., Clothiaux, E. E., Ackerman, T. P., Albrecht, B. A., Widener, K. B., Moran, K. P., et al. (2016). Development and applications of ARM millimeter-wavelength cloud radars. *Meteorological Monographs*, *57*(1), 171–1719. https://doi.org/10.1175/AMSMONOGRAPHS-D-15-0037.1

Li, J., Huang, J., Stamnes, K., Wang, T., Lv, Q., & Jin, H. (2015). A global survey of cloud overlap based on CALIPSO and CloudSat measurements. *Atmospheric Chemistry and Physics*, *15*(1), 519–536. https://doi.org/10.5194/ACP-15-519-2015

Li, J., Jian, B., Zhao, C., Zhao, Y., Wang, J., & Huang, J. (2019). Atmospheric instability dominates the long-term variation of cloud vertical overlap over the Southern Great Plains site. *Journal of Geophysical Research: Atmospheres*, *124*, 9691–9701. https://doi.org/10.1029/2019JD030954

Liang, X. Z., & Wang, W. C. (1997). Cloud overlap effects on general circulation model climate simulations. *Journal of Geophysical Research*, *102*(D10), 11039–11047. https://doi.org/10.1029/97JD00630

Lim, K. S. S., Riihimaki, L. D., Shi, Y., Flynn, D., Kleiss, J. M., Berg, L. K., et al. (2019). Long-term retrievals of cloud type and fair-weather shallow cumulus events at the ARM SGP site. *Journal of Atmospheric and Oceanic Technology*, *36*(10), 2031–2043. https://doi.org/10.1175/JTECH-D-18-0215.1

Long, C. N., Mather, J. H., & Ackerman, T. P. (2016). *The ARM tropical Western Pacific (TWP) sites. The atmospheric radiation measurement Program: The first 20 years. Meteorological Monographs* (Vol. 57, pp. 71–714). American Meteorological Society. https://doi.org/10.1175/AMSMONOGRAPH-D-15-0024.1

Mace, G., & Benson-Troth, S. (2002). Cloud-layer overlap characteristics derived from long-term cloud radar data. *Journal of Climate*, *15*(17), 2505–2515. https://doi.org/10.1175/1520-0442(2002)015<2505:CLOCDF>2.0.CO;2

Martin, S. T., Artaxo, P., Machado, L., Manzi, A. O., Souza, R. A. F., Schumacher, C., et al. (2017). The Green Ocean Amazon experiment (GoAmazon2014/5) observes pollution affecting gases, aerosols, clouds, and rainfall over the rain forest. *Bulletin of the American Meteorological Society*, *98*(5), 981–997. https://doi.org/10.1175/BAMS-D-15-00221.1

Mlawer, E. J., Taubman, S. J., Brown, P. D., Iacono, M. J., & Clough, S. A. (1997). Radiative transfer for inhomogeneous atmospheres: RRTM, a validated correlated-k model for the longwave. *Journal of Geophysical Research*, *102*(D14), 16663–16682. https://doi.org/10.1029/97JD00237

Morcrette, J. J., & Fouquart, Y. (1986). The overlapping of cloud layers in shortwave radiation parameterizations. *Journal of the Atmospheric Sciences*, *43*(4), 321–328. https://doi.org/10.1175/1520-0469(1986)043<0321:TOOCLI>2.0.CO;2

Morcrette, J. J., & Jakob, C. (2000). The response of the ECMWF model to changes in the cloud overlap assumption. *Monthly Weather Review*, *128*(6), 1707–1732. https://doi.org/10.1175/1520-0493(2000)128<1707:TROTEM>2.0.CO;2

Naud, C. M., Del Genio, A., Mace, G. G., Benson, S., Clothiaux, E. E., & Kollias, P. (2008). Impact of dynamics and atmospheric state on cloud vertical overlap. *Journal of Climate*, *21*(8), 1758–1770. https://doi.org/10.1175/2007JCLI1828.1

Neggers, R. A. J., Heus, T., & Siebesma, A. P. (2011). Overlap statistics of cumuliform boundary-layer cloud fields in large-eddy simulations. *Journal of Geophysical Research*, *116*, D21202. https://doi.org/10.1029/2011JD015650

Oreopoulos, L., Lee, D., Sud, Y. C., & Suarez, M. J. (2012). Radiative impacts of cloud heterogeneity and overlap in an atmospheric General Circulation Model. *Atmospheric Chemistry and Physics*, *12*(19), 9097–9111. https://doi.org/10.5194/ACP-12-9097-2012

Oreopoulos, L., & Norris, P. M. (2011). An analysis of cloud overlap at a midlatitude atmospheric observation facility. *Atmospheric Chemistry and Physics*, *11*(12), 5557–5567. https://doi.org/10.5194/ACP-11-5557-2011

Pincus, R., Barker, H. W., & Morcrette, J.-J. (2003). A fast, flexible, approximate technique for computing radiative transfer in inhomogeneous cloud fields. *Journal of Geophysical Research*, *108*(D13), 4376. https://doi.org/10.1029/2002JD003322

Pincus, R., Hannay, C., Klein, S. A., Xu, K. M., & Hemler, R. (2005). Overlap assumptions for assumed probability distribution function cloud schemes in large-scale models. *Journal of Geophysical Research*, *110*, D15S09. https://doi.org/10.1029/2004JD005100

Räisänen, P., Barker, H. W., Khairoutdinov, M. F., Li, J., & Randall, D. A. (2004). Stochastic generation of subgrid-scale cloudy columns for large-scale models. *Quarterly Journal of the Royal Meteorological Society*, *130*(601), 2047–2067. https://doi.org/10.1256/QJ.03.99

Shonk, J. K. P., & Hogan, R. J. (2010). Effect of improving representation of horizontal and vertical cloud structure on the Earth's global radiation budget. Part II: The global effects. *Quarterly Journal of the Royal Meteorological Society*, *136*(650), 1205–1215. https://doi.org/10.1002/QJ.646

Shonk, J. K. P., Hogan, R. J., Edwards, J. M., & Mace, G. G. (2010). Effect of improving representation of horizontal and vertical cloud structure on the Earth's global radiation budget. Part I: Review and parametrization. *Quarterly Journal of the Royal Meteorological Society*, *136*(650), 1191–1204. https://doi.org/10.1002/QJ.647

Shupe, M. D., Rex, M., Blomquist, B., Persson, O. G., Schmale, J., Uttal, T., et al. (2022). Overview of the MOSAiC expedition: Atmosphere. *Elementa: Science of the Anthropocene*, *10*(1), 00060. https://doi.org/10.1525/ELEMENTA.2021.00060

Sisterson, D. L., Peppler, R. A., Cress, T. S., Lamb, P. J., & Turner, D. D. (2016). *The ARM Southern Great Plains (SGP) site. The atmospheric radiation measurement program: The first 20 years. Meteorological Monographs* (Vol. 57, pp. 6.1–6.14). American Meteorological Society. https://doi.org/10.1175/AMSMONOGRAPHS-D-16-0004.1

Slingo, A., & Slingo, J. M. (1991). Response of the National Center for Atmospheric Research community climate model to improvements in the representation of clouds. *Journal of Geophysical Research*, *96*(D8), 15341–15357. https://doi.org/10.1029/91JD00930

Stubenrauch, C. J., Del Genio, A. D., & Rossow, W. B. (1997). Implementation of subgrid cloud vertical structure inside a GCM and its effect on the radiation budget. *Journal of Climate*, *10*(2), 273–287. https://doi.org/10.1175/1520-0442(1997)010<0273:IOSCVS>2.0.CO;2

Tian, L., & Curry, J. A. (1989). Cloud overlap statistics. *Journal of Geophysical Research*, *94*(D7), 9925–9935. https://doi.org/10.1029/JD094ID07P09925

Tompkins, A. M., & Di Giuseppe, F. (2015). An Interpretation of cloud overlap statistics. *Journal of the Atmospheric Sciences*, *72*(8), 2877–2889. https://doi.org/10.1175/JAS-D-14-0278.1

Turner, D. D., & Ellingson, R. G. (2016). *Introduction. The atmospheric radiation measurement program: The first 20 years. Meteorological Monographs* (Vol. 57, pp. v–x). American Meteorological Society. https://doi.org/10.1175/AMSMONOGRAPHS-D-16-0001.1

Varble, A. C., Nesbitt, S. W., Salio, P., Hardin, J. C., Bharadwaj, N., Borque, P., et al. (2021). Utilizing a storm-generating hotspot to study convective cloud transitions: The CACTI experiment. *Bulletin of the American Meteorological Society*, *102*(8), E1597–E1620. https://doi.org/10.1175/BAMS-D-20-0030.1

Wu, X., & Liang, X. Z. (2005). Radiative effects of cloud horizontal inhomogeneity and vertical overlap identified from a monthlong cloud-resolving model simulation. *Journal of the Atmospheric Sciences*, *62*(11), 4105–4112. https://doi.org/10.1175/JAS3565.1